MEMBRANE STRESS AND INTERNAL PRESSURE IN A RED BLOOD CELL FREELY SUSPENDED IN A SHEAR FLOW

R. TRAN-SON-TAY, S. P. SUTERA, G. I. ZAHALAK, AND P. R. RAO
Department of Mechanical Engineering, Washington University, St. Louis, Missouri 63130

ABSTRACT Presented is an algorithm for the approximate calculation of the membrane stress distribution and the internal pressure of a steadily tank-treading red cell. The algorithm is based on an idealized ellipsoidal model of the tank-treading cell (Keller, S. R., and R. Skalak, 1982, *J. Fluid Mech.*, 120:27–47) joined with experimental observations of projected length, width, and tank-treading frequency. The results are inexact because the membrane shape and velocity are assumed a priori, rather than being determined via appropriate material constitutive relations for the membrane; these results are, nevertheless, believed to be approximately correct, and show that internal pressure builds up slowly as cell elongation increases, rising more rapidly as the deformed cell approaches the limiting geometry of a prolate ellipsoid. The maximum shear stress resultant in the membrane was found to be below but approaching the yield point range at the highest shear rate applied.

INTRODUCTION

Microscopic observations of normal mammalian erythrocytes have clearly demonstrated the interesting state of motion known as "tank-treading" (Fischer and Schmid-Schönbein, 1977) in which individual cells, suspended in a shear flow, assume a stationary orientation and, driven by the surrounding flow, the membrane steadily rotates about the cytoplasmic fluid. As shown in Fig. 1, erythrocytes tank-treading steadily in a uniform shear flow present the aspect of a flattened ellipsoidal shape. This picture was taken in a device known as the rheoscope, a counter-rotating, cone-plate shear chamber which is mounted directly on the stage of an inverted microscope. (For more details, see the reference by Fischer and Schmid-Schönbein, 1977.) In addition to the cell's approximately elliptical periphery projected on the plane of shear, the translational speed of the membrane, made visible by marker beads, and thus its "tank-treading frequency" (TTF), is directly measurable.

We have been concerned with the general problem of interpreting the limited observable aspects of tank-treading motion in terms of the mechanical properties of the erythrocyte membrane. The solution to this problem rests on the availability of suitable mathematical models of the tank-treading erythrocyte. Several of the earliest attempts in this direction relied upon either the rigid ellipsoid or the liquid droplet as a model of the red cell. Later, thin shell or membrane theory was applied to liquid-filled capsule models with elastic or viscoelastic membranes. The most recent in this category by Barthès-Biesel and Sgaier (1985) is representative; the capsule is initially spherical and is limited to small deviations from its initial shape. An examination of the exact tank-treading problem as it is formulated, for example, in this paper reveals its complexity and intractability. Given (*a*) an undeformed membrane shape, (*b*) the viscosity of the internal and external fluids, (*c*) viscoelastic constitutive relations of the membrane material, and (*d*) the shear rate of the external fluid far from the membrane, it is required to determine simultaneously (*i*) the three internal and external fluid velocity components, (*ii*) the pressure, and (*iii*) the a priori unknown membrane shape (when the deformations are large), so as to satisfy (*a*) the linear equations of Stokes flow inside and outside the membrane, (*b*) the conditions of constant pressure and simple shear flow in the external fluid at infinity, (*c*) continuity of velocity across the membrane, (*d*) nonlinear relations between displacement, velocity, strain, and strain rate on the (a priori unknown) deformed membrane, and (*e*) nonlinear membrane constitutive relations between membrane stresses, strains, and strain rates. No exact solutions of this full problem, either analytical or numerical, have yet been attempted.

One way in which some progress has been made is via a semi-inverse approach wherein reasonable a priori approximations are made for the membrane shape and velocity field, and the remaining variables are solved for with much simpler linear problems. To date the most comprehensive model of the tank-treading erythrocyte is that conceived by Keller and Skalak (1982). They represent the cell by an

Dr. Tran-Son-Tay's present address is Department of Mechanical Engineering and Materials Science, Duke University, Durham, NC 27706.

Send all correspondence and requests for offprints to S. P. Sutera.

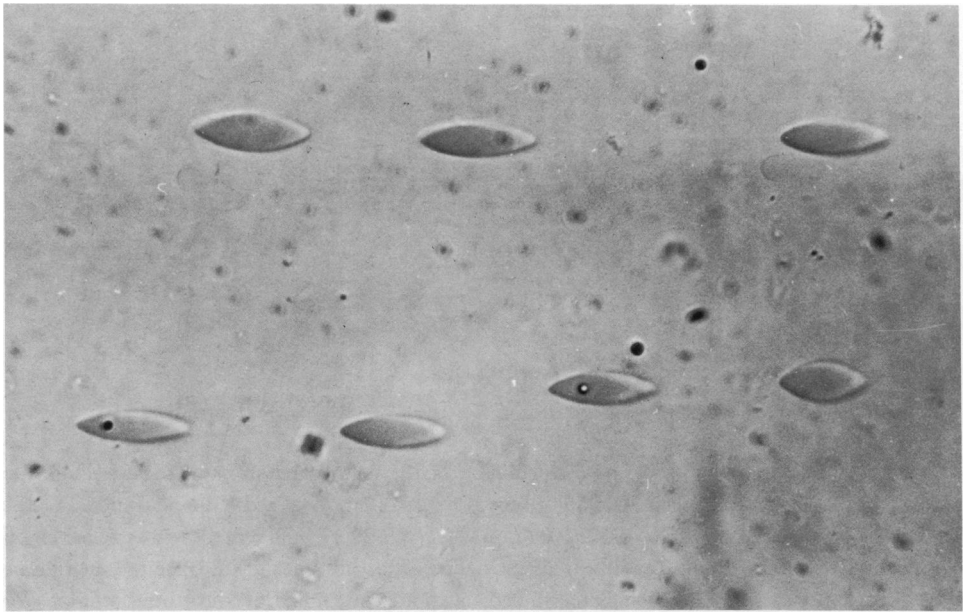

FIGURE 1 Photomicrograph of human red cells tank-treading in the rheoscope. Cells suspended in buffered saline with dextran added; viscosity = 30 cP. Applied shear rate = 200 s^{-1}. Polystyrene beads are attached to membranes of two of the cells.

ellipsoidal energy-dissipating membrane of zero thickness encapsulating an incompressible Newtonian liquid and immersed in a simple shear flow of a second incompressible Newtonian liquid. The membrane motion is prescribed in the form of a surface–velocity distribution, which is kinematically similar to that observed experimentally. Building on this model we have been able to calculate the complete external velocity field (Sutera and Tran-Son-Tay, 1983) and also develop an algorithm for determination of membrane viscosity from rheoscopic measurements of TTF and aspect ratio of the deformed cell (Tran-Son-Tay et al., 1984). In the present paper we seek the stress distribution in the membrane of the tank-treading cell; in the process it will be necessary to determine the cytoplasmic pressure. Once again we base our analysis on the Keller–Skalak (K-S) model.

MEMBRANE LOADING

Fig. 2 shows diagrammatically the model ellipsoid and defines the coordinate systems and principal flow parameters. The XYZ axes are centered in the ellipsoid and oriented such that the undisturbed shear flow has components $[\dot{\gamma}Y, 0, 0]$, where $\dot{\gamma}$ is the shear rate. The xyz axes are the principal axes of the ellipsoid whose surface is defined by

$$x^2/a^2 + y^2/b^2 + z^2/c^2 = 1. \quad (1)$$

In the K-S model the prescribed membrane–velocity field is

$$U^m = f[(a/b)y, -(b/a)x, 0], \quad (2)$$

where f is the TTF, defined here as a positive constant with dimension rad/s. The corresponding particle paths are closed ellipses lying in planes z-const., as indicated in Fig. 2 *B*, and all membrane elements orbit synchronously with the same period $T = 2\pi/f$. Membrane markers attached to tank-treading cells are in fact observed to move along paths whose projections on the XZ plane (the plane of observation) are virtually straight lines (Fischer and Schmid-Schönbein, 1977).

The membrane velocity field described by Eq. 2 does not satisfy the condition of local area conservation and, hence, does not reflect the true mechanical behavior of the red cell membrane. However, we will compute the membrane stresses from a specified distribution of surface tractions, rather than the membrane deformation. This approach will allow explicit computation of the membrane stress compo-

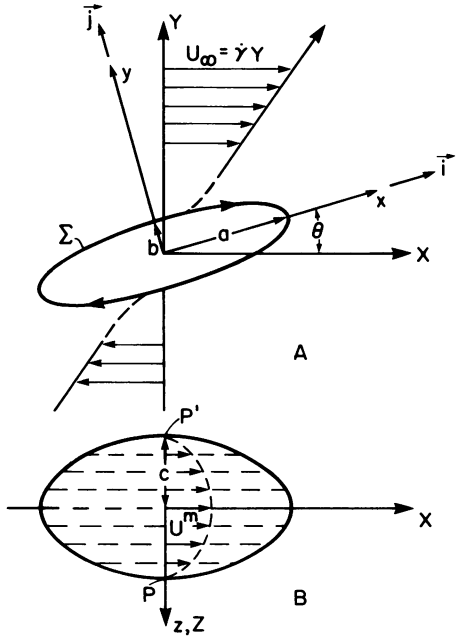

FIGURE 2 Diagram of the tank-treading ellipsoidal particle showing the notation and coordinate systems used.

nents in terms of known or observable parameters and the unknown internal pressure. To determine the latter it will be necessary to introduce the constitutive relations of the membrane material. It is also important to point out here that the use of an area-conserving velocity field will not, of itself, improve the results. Secomb and Skalak (1982) have derived two area-conserving fields on an ellipsoid. The first, with planar streamlines like those of the K-S field, predicts a longitudinal stretch ratio (λ_s), which is constant at every point on the central streamline ($z = 0$). The second had nonplanar streamlines curving away from the plane of symmetry and entailed a lower energy-dissipation rate than the first. For this reason it is probably closer to the true membrane–velocity field. It so happens that this field and the K-S field give qualitatively similar variations of λ_s along the central streamline, i.e., high at the flattest part of streamline ($x = 0$, $y = b$) and decreasing toward the points of maximum curvature ($x = \pm a$, $y = 0$). Thus, even though it fails to conserve the membrane area, the K-S field provides a description of the membrane deformation that is approximately correct.

The cartesian components of the stress exerted by the external fluid on the (outer) membrane surface Σ are expressed as

$$\tau^{o}_{ij} = -p\,\delta_{ij} + \eta_o(u^{o}_{i,j} + u^{o}_{j,i})\big|_{\Sigma} \tag{3}$$

relative to the xyz axes, where p is the external pressure, η_o is the external fluid viscosity, the u^{o}_{i} are the components of the external velocity field, and δ_{ij} is the Kronecker delta. The traction vector at any point on the outer surface of the membrane, T^o, has components defined by

$$T^{o}_{i} \equiv \tau^{o}_{ij}\, n_j, \tag{4}$$

where the n_j are the components of the outward unit normal vector, again with respect to xyz. According to Jeffery (1922), for the general triaxial ellipsoidal particle, the components of T^o reduce to

$$T^{o}_{x} = P_o\left\{-\frac{p_o x}{a^2} + \eta_o\left[\frac{8}{abc}\left(\frac{Ax}{a^2} + \frac{Hy}{b^2}\right) - \frac{4x}{a^2}(\alpha_o A + \beta_o B + \gamma_o C)\right]\right\}, \tag{5a}$$

$$T^{o}_{y} = P_o\left\{-\frac{p_o y}{b^2} + \eta_o\left[\frac{8}{abc}\left(\frac{Hx}{a^2} + \frac{By}{b^2}\right) - \frac{4y}{b^2}(\alpha_o A + \beta_o B + \gamma_o C)\right]\right\}, \tag{5b}$$

$$T^{o}_{z} = P_o\left\{-\frac{p_o z}{c^2} + \eta_o\left[\frac{8}{abc}\left(\frac{Cz}{c^2}\right) - \frac{4z}{c^2}(\alpha_o A + \beta_o B + \gamma_o C)\right]\right\}, \tag{5c}$$

where

$$P_o = \left(\frac{x^2}{a^4} + \frac{y^2}{b^4} + \frac{z^2}{c^4}\right)^{-1/2}, \tag{6}$$

and the remaining coefficients, A, B, C, H, α_o, β_o, and γ_o are expressible in terms of elliptic integrals. The constant p_o is the remote pressure far from the ellipsoid. These coefficients were all derived in the paper by Sutera and Tran-Son-Tay (1983); for the reader's convenience they are repeated in the Appendix.

The internal fluid is driven in a closed circulatory pattern by the tank-treading membrane. The corresponding velocity field is given by the surface velocity, Eq. 2, extended into the interior of the ellipsoid (Keller and Skalak, 1982), i.e.,

$$u^{i} = f[(a/b)y, -(b/a)x, 0]. \tag{7}$$

Associated with this velocity field is a uniform internal pressure p_i. The stress exerted over the internal surface of the membrane by the internal fluid has components

$$\tau^{i}_{ij} = -p_i\delta_{ij} + \eta_i(u^{i}_{i,j} + u^{i}_{j,i})\big|_{\Sigma}, \tag{8}$$

where η_i is the viscosity of the internal fluid. The components of the corresponding stress vector T^i are

$$T^{i}_{x} = P_o\left\{\frac{p_i x}{a^2} - \eta_i f\left(\frac{a}{b} - \frac{b}{a}\right)\frac{y}{b^2}\right\}, \tag{9a}$$

$$T^{i}_{y} = P_o\left\{\frac{p_i y}{b^2} - \eta_i f\left(\frac{a}{b} - \frac{b}{a}\right)\frac{x}{a^2}\right\}, \tag{9b}$$

$$T^{i}_{z} = \frac{P_o p_i z}{c^2}. \tag{9c}$$

Now the resultant stress vector at any point on the moving membrane is the vector sum $T = T^o + T^i$ whose components reduce to

$$T_x = P_o\left\{\left(D + \frac{8A\eta_o}{abc}\right)\frac{x}{a^2} + \left(\frac{8H\eta_o}{abc} - E\right)\frac{y}{b^2}\right\}, \tag{10a}$$

$$T_y = P_o\left\{\left(\frac{8\eta_o H}{abc} - E\right)\frac{x}{a^2} + \left(D + \frac{8B\eta_o}{abc}\right)\frac{y}{b^2}\right\}, \tag{10b}$$

$$T_z = P_o\left(D + \frac{8\eta_o C}{abc}\right)\frac{z}{c^2}, \tag{10c}$$

where

$$D = p_i - p_o - 4\eta_o(\alpha_o A + \beta_o B\ \gamma_o C), \tag{11}$$

and

$$E = \eta_i f(a/b - b/a). \tag{12}$$

MEMBRANE STRESS DISTRIBUTION

In this model we assume that the mass of the thin ellipsoidal membrane is negligible and ignore bending

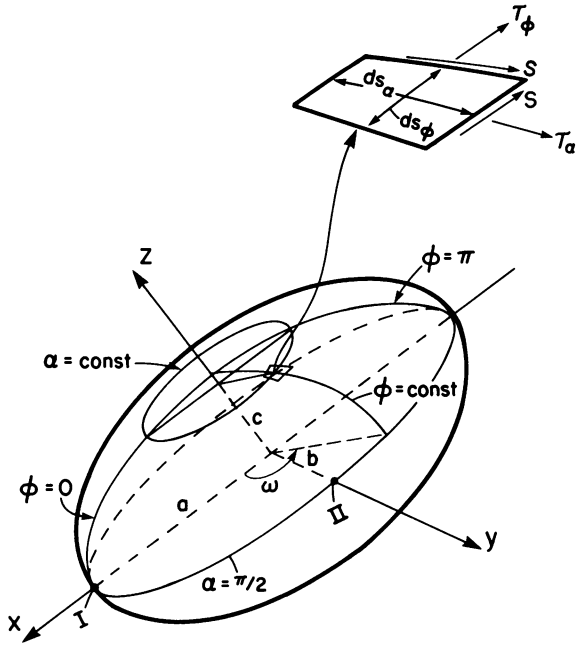

FIGURE 3 Diagram illustrating membrane stress components in the ellipsoidal membrane.

stresses within the membrane. Then the state of stress at any point in the membrane is defined by two in-plane normal stresses and an in-plane shear stress. At each instant of time, each element of the membrane must be in a state of equilibrium, and the internal stress distribution is completely determined by the applied surface loading T. The ellipsoidal surface of the membrane can be expressed in terms of two surface coordinates, ϕ and α, as

$$\left.\begin{aligned} x &= a \sin\alpha \cos\phi, \\ y &= b \sin\alpha \sin\phi, \\ z &= c \cos\alpha. \end{aligned}\right\} \tag{13}$$

Note that this is not an orthogonal surface-coordinate system.

The sketch in Fig. 3 shows a curvilinear surface element with edges of length ds_α and ds_ϕ parallel to the ϕ- and α-coordinate curves, respectively, whereon the surface stress resultants[1] (force per unit length) are denoted by T_α, T_ϕ, and S. Note that T_α and T_ϕ represent forces acting, respectively, along the local directions of the ϕ- and α-coordinate curves. Direct solution for these components from the fundamental equations of membrane equilibrium is complicated by the ellipsoidal geometry. We circumvent this difficulty by resorting to a transformation method (Novozhilov, 1964). By linear coordinate transformation the ellipsoidal membrane of interest can be mapped onto a sphere. A surface loading related to that which acts over the ellipsoid is then specified for the sphere and the easier problem of calculating the stress resultants in the spherical membrane solved. The latter resultants, operated on by an appropriate linear transformation, give finally the stress resultants in the ellipsoidal membrane.

Consider a general linear coordinate transformation of the form:

$$x = c_1 x^*, y = c_2 y^*, z = c_3 z^*, \tag{14}$$

where $x^* y^* z^*$ are the transformed coordinates, also cartesian, and the coefficients c_1, c_2, c_3 are constants. This transformation will map the ellipsoid, Eq. 13, onto a sphere of radius c, Fig. 4, if we take

$$c_1 = a/c, c_2 = b/c, c_3 = 1. \tag{15}$$

The polar equations of this sphere, analogous to Eqs. 13, are

$$\left.\begin{aligned} x^* &= c \sin\alpha \cos\phi, \\ y^* &= c \sin\alpha \sin\phi, \\ z^* &= c \cos\alpha. \end{aligned}\right\} \tag{16}$$

We need further to introduce the direction cosines, with respect to the fixed cartesian system, of the two edges and the outward normal of the surface element $ds_\alpha^* \, ds_\phi^*$ sketched in Fig. 4. These will be denoted l_1, l_2, l_3 for ds_α^*, m_1, m_2, m_3 for ds_ϕ^*, and n_1, n_2, n_3 for the normal. In terms of the polar angles α and ϕ they are

$$\left.\begin{aligned} (l_1, l_2, l_3) &= (\cos\alpha \cos\phi, \cos\alpha \sin\phi, -\sin\alpha), \\ (m_1, m_2, m_3) &= (-\sin\phi, \cos\phi, 0), \\ (n_1, n_2, n_3) &= (\sin\alpha \cos\phi, \sin\alpha \sin\phi, \cos\alpha). \end{aligned}\right\} \tag{17}$$

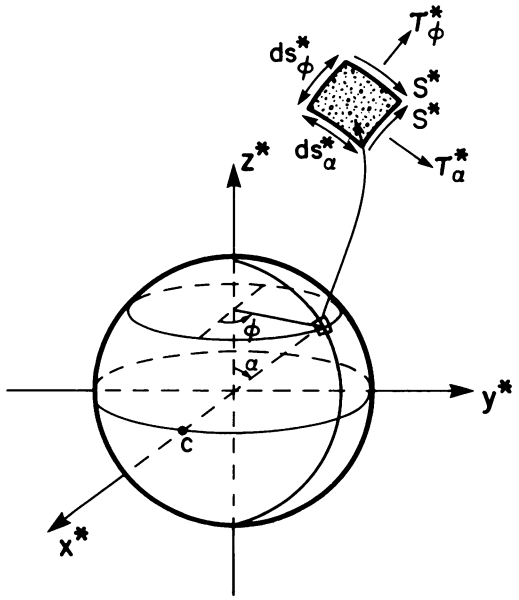

FIGURE 4 Spherical transform of the ellipsoidal membrane of Fig. 3.

[1]In the ensuing text the abbreviated terminology "stress" is occasionally used to stand for "stress resultant."

According to Novozhilov the surface loading on the transformed membrane, i.e., the sphere, denoted T^*, must be related to the surface loading T on the original ellipsoidal membrane as follows:

$$(T_x, T_y, T_z) = \frac{(c_1 T_x^*, c_2 T_y^*, c_3 T_z^*)}{\sqrt{c_2^2 c_3^2 n_1^2 + c_3^2 c_1^2 n_2^2 + c_1^2 c_2^2 n_3^2}}. \tag{18}$$

Insertion of the definitions for c_1, c_2, c_3 (Eq. 15) and for n_1, n_2, n_3 (Eq. 17) into this relationship leads to considerable simplification and yields

$$T_x^*, T_y^*, T_z^* = \frac{b}{P_o} T_x, \frac{a}{P_o} T_y, \frac{ab}{cP_o} T_z, \tag{19}$$

where the components T_x, T_y, and T_z are as previously defined (Eqs. 10a–c).

The next step is to solve for the resultants T_α^*, T_ϕ^*, and S^* in the spherical membrane corresponding to the loading specified by Eq. 19. The three components are governed by the classical differential equations of equilibrium for a membrane in the shape of a surface of revolution:

$$\left.\begin{aligned} &\frac{\partial T_\alpha^*}{\partial \alpha} + (T_\alpha^* - T_\phi^*)\cot\alpha + \frac{1}{\sin\alpha}\frac{\partial S^*}{\partial \phi} + c q_\alpha^* = 0, \\ &\frac{\partial S^*}{\partial \alpha} + 2S^* \cot\alpha + \frac{1}{\sin\alpha}\frac{\partial T_\phi^*}{\partial \phi} + c q_\phi^* = 0, \\ &T_\alpha^* + T_\phi^* = c q_n^*, \end{aligned}\right\} \tag{20}$$

where q_α^*, q_ϕ^*, and q_n^* are the spherical components of the surface load vector T^*. These components are related to the cartesian components T_x^*, T_y^*, T_z^* through the direction cosines of the surface element edges and normal:

$$\left.\begin{aligned} q_\alpha^* &= l_1 T_x^* + l_2 T_y^* + l_3 T_z^*, \\ q_\phi^* &= m_1 T_x^* + m_2 T_y^* + m_3 T_z^*, \\ q_n^* &= n_1 T_x^* + n_2 T_y^* + n_3 T_z^*. \end{aligned}\right\} \tag{21}$$

For the sake of conciseness here, the complete expressions for q_α^*, q_ϕ^*, and q_n^* have been placed in the Appendix. Examination of these expressions verifies that they are periodic functions of ϕ with period π, and each component is expressible as a three-term finite Fourier series of the form

$$q_\alpha^* = q_{\alpha,0} + q_{\alpha,2}\cos 2\phi + q'_{\alpha,2}\sin 2\phi, \tag{22}$$

and similarly for q_ϕ^* and q_n^*. The corresponding set of nine coefficients is also listed in the Appendix.

It follows from the periodicity of the surface loading that the stress resultants in the spherical membrane, T_α^*, T_ϕ^*, and S^*, must be similarly periodic. Hence, we introduce into the partial differential Eqs. 20 expansions of the form

$$T_\alpha^* = T_{\alpha,0} + T_{\alpha,2}\cos 2\phi + T'_{\alpha,2}\sin 2\phi, \tag{23}$$

where the coefficients are functions of α alone. Substitution of Eq. 23 and similar expansions for T_ϕ^* and S^* into Eqs. 20 reduces these to a set of ordinary differential equations in the coefficients as functions of α. Tran-Son-Tay (1983) has solved these equations, subject to appropriate boundary conditions, and obtained

$$T_\alpha^* = (D + 8\eta_o C/abc)ab/2c + cG\cos 2\phi + cL\sin 2\phi, \tag{24a}$$

$$T_\phi^* = cF\sin^2\alpha + (D + 8\eta_o C/abc)ab/2c - cG\cos^2\alpha\cos 2\phi - cL\cos^2\alpha\sin 2\phi, \tag{24b}$$

$$S^* = cL\cos\alpha\cos 2\phi - cG\cos\alpha\sin 2\phi, \tag{24c}$$

wherein all the coefficients are defined in the Appendix.

According to Novozhilov (1964), the stress resultants in the ellipsoidal membrane are related to those in the spherical membrane as follows:

$$T_\alpha = \left\{\frac{c_1^2 l_1^2 + c_2^2 l_2^2 + c_3^2 l_3^2}{c_1^2 m_1^2 + c_2^2 m_2^2 + c_3^2 m_3^2}\right\}^{1/2} T_\alpha^*, \tag{25a}$$

$$T_\phi = \left\{\frac{c_1^2 m_1^2 + c_2^2 m_2^2 + c_3^2 m_3^2}{c_1^2 l_1^2 + c_2^2 l_2^2 + c_3^2 l_3^2}\right\}^{1/2} T_\phi^*, \tag{25b}$$

$$S = S^*, \tag{25c}$$

where the c_i, l_i, and m_i are defined in Eqs. 15 and 17. Inserting these definitions, we find for T_α and T_ϕ

$$T_\alpha = \left\{\frac{a^2\cos^2\alpha\cos^2\phi + b^2\cos^2\alpha\sin^2\phi + c^2\sin^2\alpha}{a^2\sin^2\phi + b^2\cos^2\phi}\right\}^{1/2} T_\alpha^*, \tag{26a}$$

$$T_\phi = \left\{\frac{a^2\sin^2\phi + b^2\cos^2\phi}{a^2\cos^2\alpha\cos^2\phi + b^2\cos^2\alpha\sin^2\phi + c^2\sin^2\alpha}\right\}^{1/2} T_\phi^*. \tag{26b}$$

These equations, coupled with the solutions, Eqs. 24a–c, thus determine the stress everywhere in the membrane of the arbitrary ellipsoid symmetrically oriented and tank-treading in a simple shear flow. Note that once the shape of the membrane is assumed as known and the surface loading is given, the internal stress distribution in the membrane is statically determinate and independent of any particular assumptions about the material properties of the membrane.

INTERNAL PRESSURE

Careful scrutiny of the expressions obtained for the membrane stress resultants T_α, T_ϕ, and S shows that they contain several parameters, all but one of which are either known a priori, e.g., η_i, η_o, or observable in the tank-treading motion, e.g., f, $a\cos\theta$, c. The exception is the internal pressure, p_i. While it is generally accepted that the red cell membrane supports no pressure difference in the resting state (Fung, 1966), transmembrane pressure differences must be expected in the case of the tank-treading cell. Therefore, p_i is an additional unknown that must be found simultaneously with the stress components. To accomplish this it is necessary to invoke the constitutive relations of the membrane.

The maximum shear stress resultant at any point on the

membrane, S_{max}, is defined as one-half the magnitude of the difference between the principal normal stresses, T_1 and T_2, at that point,

$$S_{max} \equiv \tfrac{1}{2}|T_1 - T_2|. \tag{27}$$

As a first approximation, it is common to represent the membrane material as a Kelvin–Voigt viscoelastic solid. For an area-conserving material of this type, the maximum shear stress at any point can be expressed in terms of a principal extension ratio, λ, at that point as (Evans and Skalak, 1980)

$$S_{max} = \left| \frac{\mu_m}{2}(\lambda^2 - \lambda^{-2}) + 2\eta_m \frac{d}{dt}(\ln \lambda) \right|. \tag{28}$$

In the right member of this equation the first term is the elastic contribution with μ_m, the membrane shear modulus of elasticity, whereas the second term is the viscous contribution with η_m, the membrane coefficient of shear viscosity. The operator d/dt signifies the material time derivative.

Assume that the unstressed configuration of the material strip C is the meridian strip C_o, as sketched in Fig. 5 *b*, and let σ and s denote arc lengths measured along C_o and C, respectively. There must be a one-to-one time-dependent mapping between the moving points on C and their original coordinates on C_o. This mapping is expressed by

$$s = s(\sigma, t) \text{ or } \sigma = \sigma(s, t). \tag{29}$$

The speed of points on the moving membrane strip can be expressed as

$$v_m = (\partial s/\partial t)_\sigma, \tag{30}$$

and the longitudinal extension ratio of material elements comprising C as

$$\lambda_s = (\partial s/\partial \sigma)_t. \tag{31}$$

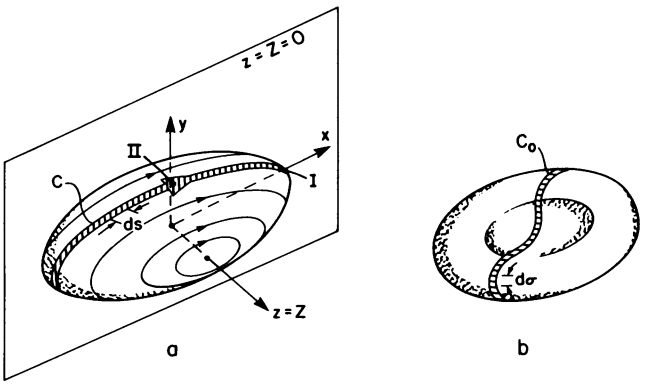

FIGURE 5 Sketches illustrating midplane contour C on tank-treading ellipsoidal membrane (*a*) and assumed unstressed configuration of same contour (*b*).

Combination of Eqs. 30 and 31 leads to a Maxwell-type relation:

$$(\partial \lambda_s/\partial t)_\sigma = (\partial v_m/\partial \sigma)_t. \tag{32}$$

Next we note that

$$\frac{d}{dt}(\ln \lambda_s) = \frac{1}{\lambda_s}\left(\frac{\partial \lambda_s}{\partial t}\right)_\sigma = \left(\frac{\partial \sigma}{\partial s}\right)_t \cdot \left(\frac{\partial v_m}{\partial \sigma}\right)_t = \left(\frac{\partial v_m}{\partial s}\right)_t. \tag{33}$$

From the symmetry of the assumed K-S surface velocity field it is clear that $(\partial v_m/\partial s)_t$ vanishes, and so, therefore, does the viscous contribution to the maximum shear stress, at four particular points, viz. $x = \pm a$, $y = z = 0$ and $y = \pm b$, $x = z = 0$ (Fig. 2) or, equivalently, $\alpha = \pi/2$, $\phi = 0$, $\pi/2$, π and $3\pi/2$ (Fig. 3). Thus, at these locations the maximum shear resultant reduces to

$$S_{max} = \mu/2\,|\lambda_s^2 - \lambda_s^{-2}|. \tag{34}$$

We proceed next to evaluate the stress resultants T_α and T_ϕ at the two points $\alpha = \pi/2$, $\phi = 0$ and $\alpha = \pi/2$, $\phi = \pi/2$ by insertion of these coordinates into Eqs. 24a, 24b, 26a, and 26b. At these points T_α and T_ϕ are also principal stresses so that

$$S_{max} = \tfrac{1}{2}|T_\alpha - T_\phi|. \tag{35}$$

Denoting the extension ratio λ_s at the same points as λ_I and λ_{II}, respectively, we arrive at

$$|(a/2 - ab^2/2c^2)(D + 8\eta_o C/abc) + c^2 G/b - bF| = \mu|\lambda_I^2 - \lambda_I^{-2}|, \tag{36}$$

$$|(b/2 - a^2 b/2c^2)(D + 8\eta_o C/abc) - c^2 G/a - aF| = \mu|\lambda_{II}^2 - \lambda_{II}^{-2}|. \tag{37}$$

Recall that the pressure p_i is embedded in the coefficient D, Eq. 11. Eqs. 36 and 37 thus contain three unknowns: p_i, λ_I, and λ_{II}. Another condition is therefore necessary to render the problem determinate. This is provided by a kinematic condition on the material strip comprising the contour C.

For the steady-state motion being considered here, the configuration of strip C does not change with time so that

$$(\partial \lambda_s/\partial t)_s = 0, \tag{38}$$

whence

$$(\partial \lambda_s/\partial t)_\sigma = (\partial \lambda_s/\partial s)_t (\partial s/\partial t)_\sigma = (\partial \lambda_s/\partial s)_t\, v_m, \tag{39}$$

and

$$(\partial v_m/\partial \sigma)_t = (\partial v_m/\partial s)_t (\partial s/\partial \sigma)_t = (\partial v_m/\partial s)_t \lambda_s. \tag{40}$$

As a consequence of the relation, Eq. 32, we equate the right members of Eqs. 39 and 40 to get

$$v_m(\partial \lambda_s/\partial s)_t = \lambda_s(\partial v_m/\partial s)_t, \tag{41}$$

a differential equation that can be integrated at any instant of time. Separating variables and integrating, we obtain

$$\frac{1}{\lambda_s}\frac{d\lambda_s}{ds} = \frac{1}{v_m}\frac{dv_m}{ds},$$

$$\ln \lambda_s = \ln v_m + \text{const.},$$

$$\lambda_s = K v_m, \tag{42}$$

where K is a constant of integration. Note that this simple equation is completely general and holds for any mathematical model of a steadily tank-treading membrane.

The constant K can be determined from Eq. 42 and the assumed Keller–Skalak surface–velocity field. First we note that the membrane speed v_m at any point on the contour C is given by (Eq. 2)

$$v_m = f\sqrt{(a^2y^2/b^2) + (b^2x^2/a^2)}. \tag{43}$$

Thus,

$$\lambda_s = \left(\frac{\partial s}{\partial \sigma}\right)_t = Kf\sqrt{(a^2y^2/b^2) + (b^2x^2/a^2)},$$

whence

$$d\sigma = \frac{ds}{Kf\sqrt{(a^2y^2/b^2) + (b^2x^2/a^2)}}. \tag{44}$$

Now, on the elliptical contour C,

$$ds = \sqrt{1 + \left(\frac{dy}{dx}\right)^2}\,dx = \left[\left(\frac{a^2y^2}{b^2} + \frac{b^2x^2}{a^2}\right)\Big/\frac{a^2y^2}{b^2}\right]^{1/2} dx,$$

which, when substituted into Eq. 44, gives

$$d\sigma = \frac{b\,dx}{Kfay} = \frac{dx}{Kf\sqrt{a^2 - x^2}}. \tag{45}$$

Integrating this from $x = 0$ to $x = a$, i.e., over a quarter of the contour C, we find

$$C_o/4 = \pi/2Kf, \tag{46}$$

where $C_o/4$ denotes a length equal to one-quarter of the unstressed contour C_o. It follows that

$$K = 2\pi/fC_o. \tag{47}$$

Note that combination of Eqs. 42, 43, and 47 yields an expression of the extension ratio at any point of the contour C. At the particular points $x = a$, y = 0 and $x = 0$, $y = b$,

$$\lambda_I = \lambda(a,0) = 2\pi b/C_o, \tag{48}$$

$$\lambda_{II} = \lambda(0,b) = 2\pi a/C_o. \tag{49}$$

For a typical human erythrocyte tank-treading at a moderate shear rate we typically observe $a = 6$ and $b = 1.5$ μm. If we assume $C_o = 18$ μm, approximately, we calculate

$$\lambda_I = 0.52 \text{ and } \lambda_{II} = 2.1,$$

numbers that appear reasonable. It is interesting to note that the material element located at the "nose" of the ellipsoidal cell (point I) is shortened rather than stretched ($\lambda_I < 1$) in the direction of motion. At this point, then, the extension ratio in the transverse direction must be 1/0.52 = 1.92, indicating stretching in the transverse direction.

To recapitulate, Eqs. 48 and 49, coupled with experimental data for a and b along with a reasonable average value for C_o, give us the elongation ratios, λ_I and λ_{II}. The values so calculated can then be taken to either of Eqs. 36 and 37, respectively, each of which is thus reduced to an equation in one remaining unknown, p_i. To solve for p_i, of course, the membrane elastic modulus μ_m must also be provided.

EXPERIMENTAL DATA

In a study of the effect of aging on the deformability of human erythrocytes (Sutera et al., 1985), we subjected the top (~ young) and bottom (~ old) 10% fractions of density-separated cells from 10 normal donors to graded levels of shear rate in a rheoscope. At each shear rate the projected length ($2a\cdot\cos\theta$) and width ($2c$) were measured on 30–40 cells from each donor; these measurements were

TABLE I
EXPERIMENTAL DATA: NORMAL HUMAN RBC

	Top 10%			Bottom 10%		
$\dot{\gamma}$	$(a\cos\theta)$*	c*	N‡	$(a\cos\theta)$*	c*	N‡
s^{-1}	μm	μm		μm	μm	
28.6	5.42 ± 0.54	3.42 ± 0.27	392	4.80 ± 0.44	3.52 ± 0.24	341
114.3	6.81 ± 0.64	2.71 ± 0.24	321	5.78 ± 0.73	2.84 ± 0.27	434
171.4	7.15 ± 0.64	2.55 ± 0.21	314	6.14 ± 0.81	2.66 ± 0.25	332
228.6	7.35 ± 0.69	2.45 ± 0.22	314	6.41 ± 0.79	2.56 ± 0.27	401
285.7	7.62 ± 0.56	2.38 ± 0.22	284	6.44 ± 0.82	2.51 ± 0.26	339
457.2	7.80 ± 0.72	2.00 ± 0.21	24	7.48 ± 0.54	2.21 ± 0.17	33

*Uncorrected lengths. Mean ± SD.
‡Number of cells, pooled from 8 to 10 donors.

then pooled and averaged (see Table I). The indicated shear rates correspond to nominal gap shear stresses of 10, 40, 60, 80, 100, and 160 dyn/cm^2 at a suspending viscosity of 35 cP.

The averages presented in Table I were first used as inputs for computations of corrected ellipsoid dimensions (semi-axes *a, b, c*) and the angle of inclination, θ, as described previously (Tran-Son-Tay et al., 1984) (see Table II). For this purpose the membrane area S and the cell volume V were assigned the average values indicated. These values are based on the surface measurements of Linderkamp and Meiselman (1982) and the volume measurements of Nash and Meiselman (1983). The tank-treading frequency, f, also required for these computations, was not measured independently here. Recall that f is proportional to the applied shear rate, $\dot{\gamma}$. Hence, we calculated f for each $\dot{\gamma}$ using the slope functions generated in our earlier study of TTF in fractionated populations of normal red cells tank-treading in the same suspending medium, viz., $f/\dot{\gamma} = 0.211$ (young cells) and 0.181 (old cells) (Sutera et al., 1983). The corrected geometrical quantities in Table II were finally used to compute the longitudinal extension ratio, λ_s, and the membrane stress resultants, T_α and T_ϕ, along the central streamline ($\alpha = p/2$) of the tank-treading membrane. For this purpose we set $\mu_m = 6 \times 10^{-3}$ dyn/cm. The internal pressure was also computed at the points of maximum (I) and minimum (II) curvature on the same streamline.

COMPUTED RESULTS

Fig. 6, corresponding to average parameters of the young and old cells, displays the computed values of T_α, T_ϕ, and λ_s as functions of the polar angle $\omega = \tan^{-1}(b\tan\phi/a)$ (see Fig. 3) on the central streamline, $\alpha = \pi/2$, for one shear rate, 286 s^{-1}. As indicated in Fig. 3, T_α is the stress resultant transverse to the streamline and T_ϕ is the component parallel to it. For all six shear rates the internal pressure, p_i, was computed at point I from Eq. 36 and at point II from Eq. 37. The differences between p_i and the remote external pressure, p_o, termed the cytoplasmic overpressure, are presented in Table III, along with the average of the two differences. These averaged estimates for the cytoplasmic overpressure are also displayed as points for the young and old cell geometries, respectively, in Fig. 7, together with a curve indicating the mean variation of this parameter with shear rate.

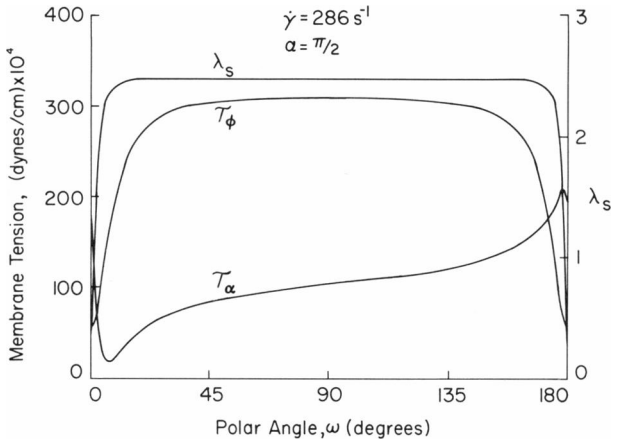

FIGURE 6 Distributions of principal membrane stress resultants and longitudinal elongation ratio along central streamline ($\alpha = \pi/2$) of tank-treading membrane. From computations based on measured deformations of normal cells tank-treading at shear rate of 286 s^{-1}. The cell dimensions used in this calculation were averages of the old-cell and young-cell dimensions listed in Table II, and f is 56 rad/s^{-1}. The mean cytoplasmic overpressure $\overline{\Delta p}$, and the membrane shear modulus, μ_m, were taken as 86 dyn/cm^2 and 6×10^{-3} dyn/cm, respectively. Points I and II seen in Figs. 3 and 5 correspond to $\phi = 0$ and 90°, respectively.

DISCUSSION

The results given in Table III and Fig. 7 show that Eqs. 36 and 37 yield different values of p_i, in apparent conflict with the underlying K-S model, which calls for uniform pressure in the interior (cytoplasmic) flow. This finding points out a fundamental inconsistency in the present analysis, viz., that the membrane shape and velocity field, rather than being treated as unknown, to be determined by the viscous flow equations, the equations of membrane equilibrium, and the membrane constitutive relations, have been specified a priori. Forcing this approximate geometry and

TABLE II
COMPUTED GEOMETRICAL PARAMETERS*

	Top 10%				Bottom 10%			
	$S = 148\ \mu m^2$, $V = 96\ \mu m^3$, $(f/\dot{\gamma}) = 0.211$				$S = 117.5\ \mu m^2$, $V = 82\ \mu m^3$, $(f/\dot{\gamma}) = 0.181$			
$\dot{\gamma}$	*a*	*b*	*c*	θ	*a*	*b*	*c*	θ
28.6	5.79	1.11	3.58	12.0	4.65	1.26	3.35	10.5
114.3	7.16	1.15	2.78	12.4	5.57	1.31	2.69	10.3
171.4	7.51	1.17	2.61	12.3	5.86	1.34	2.50	10.2
228.6	7.72	1.18	2.52	12.3	6.05	1.36	2.38	10.0
285.7	7.93	1.19	2.42	12.1	6.11	1.37	2.35	10.1
457.2	8.57	1.25	2.15	12.5	6.70	1.50	1.95	9.2

*a, b, c in microns; θ in degrees.

TABLE III
COMPUTED RESULTS: CYTOPLASMIC OVERPRESSURE*

	Top 10%			Bottom 10%		
$\dot{\gamma}$	Δp_I	Δp_{II}	$\overline{\Delta p}^\ddagger$	Δp_I	Δp_{II}	$\overline{\Delta p}^\ddagger$
28.6	7	−25	−18	14	−41	−13.5
114.3	52	−1	25.5	60	−13	23.5
171.4	73	13	43	85	0	42.5
228.6	94	28	61	109	14	61.5
285.7	115	43	79	133	28	80.5
457.2	209	108	158.5	304	120	212

*Δp, internal pressure − remote external pressure, dyn/cm^2; subscripts I and II signify correspondence to points I and II, Fig. 5.
‡Arithmetic average of Δp_I and Δp_{II}.

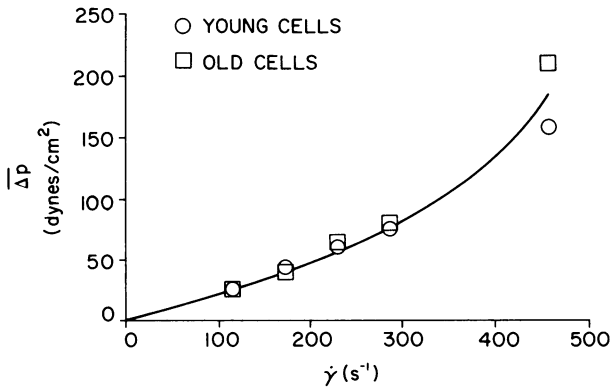

FIGURE 7 Increase of mean internal pressure with shear rate, calculated from measured dimensions for young cells and old cells.

velocity field on the membrane equations must be expected to entail errors in the resulting distributions of membrane stress as well as the internal pressure. While the ellipsoidal shape together with the K-S surface–velocity distribution demand a constant internal pressure, there is no reason to suppose that this is strictly true in a real tank-treading cell. (It should be understood that a nonuniform pressure within the cell will result in a nonlinear cytoplasmic velocity field. However, an approximate, worst case analysis indicates that the assumption of a linear velocity profile would result in an error of not more than 30% in the calculated local membrane traction on the inner membrane surface.) In view of the uncertainties inherent in the averaged experimental data, which are the basis for these results, and also the idealized nature of the K-S model, the discrepancies do not seem great. That the calculated overpressure is always smaller at the minimum curvature point (II) could perhaps be expected. The negative values obtained at the two lowest shear rates are considered as insignificant, suggesting simply that the overpressure is negligible until the overall elongation of the cell is sufficiently great. What is more interesting is the rate at which the average overpressure builds up as the shear rate and cell elongation increase. Noting that the limiting elongation is constrained by the transition from a triaxial to a biaxial (prolate) ellipsoid, i.e., $b \rightarrow c$, we see that the cells are approaching this limit at the highest shear rate of 457 s^{-1} (see Table II). The corresponding mean overpressure is 185 dyn/cm^2. This is still well below the 1,252 dyn/cm^2 given by Skalak (1973) for an osmotically sphered red cell.

The stress resultants plotted in Fig. 6 are seen to be of order 10^{-2} dyn/cm. On the central streamline T_α and T_ϕ are principal stresses so that the maximum shear stress resultant, Eq. 35, is readily estimated. We see from the curves of Fig. 6 that S_{max} reaches a maximum of $\sim 2 \times 10^{-2}$ dyn/cm in the vicinity of the high curvature points, $\phi = 0, 180$, which is at the lower end of the accepted yield point range, 2–8 $\times$ 10^{-2} dyn/cm (Evans and Hochmuth, 1978). Another interesting aspect of the plots of Fig. 6 is the difference in the variation of T_α and T_ϕ. The latter exhibits symmetry about the point of $\phi = 90°$, reflecting the variation of the longitudinal elongation, λ_s, while T_α exhibits an unsymmetrical variation with local maxima near the leading and trailing tips, opposite to T_ϕ, which has minima at these points.

CONCLUSION

In summary, we have estimated the membrane stresses and the internal pressure generated in a red blood cell that is freely suspended in shear flow. The estimations are based on rheoscopic observations of the deformation of individual cells in steady-state tank-treading. We have shown that the internal pressure at first builds up slowly as the cell elongation increases, but then rises rapidly as the deformed cell approaches the limiting geometry of a prolate ellipsoid. The maximum shear stress resultant in the membrane was found to be below but approaching the yield point range for the shear rates applied here.

APPENDIX

Coefficients Appearing in Eqs. 5a–c

$$A = (\alpha_o'' + \beta_o''/2)\dot{\gamma} \sin 2\theta/6(\alpha_o''\beta_o'' + \beta_o''\gamma_o'' + \gamma_o''\alpha_o''), \quad \text{(A1)}$$

$$B = -(\beta_o'' + \alpha_o''/2)\dot{\gamma} \sin 2\theta/6(\alpha_o''\beta_o'' + \beta_o''\gamma_o'' + \gamma_o''\alpha_o''), \quad \text{(A2)}$$

$$C = -(\alpha_o'' - \beta_o'')\dot{\gamma} \sin 2\theta/12(\alpha_o''\beta_o'' + \beta_o''\gamma_o'' + \gamma_o''\alpha_o''), \quad \text{(A3)}$$

$$H = \frac{\alpha_0[\tfrac{1}{2}\dot{\gamma}\cos 2\theta - f(a^2 - b^2)/2ab] - b^2\gamma_0'[-\dot{\gamma}/2 + f(a^2 + b^2)/2ab]}{2(a^2\alpha_0 + b^2\beta_0)\gamma_0'}. \quad \text{(A4)}$$

The following integral identities are valid for the case $a > c > b$:

$$\alpha_o \equiv \int_0^\infty \frac{ds}{(a^2 + s)\Delta(s)} = \frac{2[F(\nu, q) - E(\nu, q)]}{(a^2 - c^2)\sqrt{a^2 - b^2}}, \quad \text{(A5)}$$

$$\beta_o \equiv \int_0^\infty \frac{ds}{(b^2 + s)\Delta(s)} = -\frac{2E(\nu, q)}{(c^2 - b^2)\sqrt{a^2 - b^2}} + \frac{2}{c^2 - b^2}\sqrt{\frac{(\lambda + c^2)}{(\lambda + b^2)(\lambda + a^2)}}, \quad \text{(A6)}$$

$$\gamma_o \equiv \int_0^\infty \frac{ds}{(c^2 + s)\Delta(s)} = \frac{2E(\nu, q)\sqrt{a^2 - b^2}}{[(c^2 - b^2)(a^2 - c^2)]} - \frac{2F(\nu, q)}{(a^2 - c^2)\sqrt{a^2 - b^2}} - \frac{2}{c^2 - b^2}\sqrt{\frac{\lambda + b^2}{(\lambda + c^2)(\lambda + a^2)}}, \quad \text{(A7)}$$

where s is a running variable and

$$\Delta(s) \equiv \{(a^2 + s)(b^2 + s)(c^2 + s)\}^{1/2}, \quad \text{(A8)}$$

$$F(\nu, q) \equiv \int_0^\nu \frac{d\theta}{\sqrt{1 - q^2 \sin^2\theta}}, \quad \text{(A9)}$$

$$E(\nu, q) \equiv \int_0^\nu \sqrt{1 - q^2 \sin^2\theta}\, d\theta, \quad \text{(A10)}$$

$$\nu \equiv \arcsin \sqrt{(a^2 - b^2)/(a^2 + \lambda)}, \tag{A11}$$

$$q \equiv \sqrt{(a^2 - c^2)/(a^2 - b^2)}. \tag{A12}$$

The primed and double-primed quantities appearing in the foregoing equations are defined as linear combinations of α_o, β_o, and γ_o:

$$\gamma_o' \equiv (\beta_o - \alpha_o)/(a^2 - b^2), \tag{A13}$$

$$\alpha_o'' \equiv \frac{b^2\beta_o - c^2\gamma_o}{b^2 - c^2},\ \beta_o'' \equiv \frac{c^2\gamma_o - a^2\alpha_o}{c^2 - a^2},$$

$$\gamma_o'' \equiv \frac{a^2\alpha_o - b^2\beta_o}{a^2 - b^2}. \tag{A14}$$

Spherical Components of Surface Load Vector T^*

$$\begin{aligned} q_\alpha^* = {} & \tfrac{1}{2}\{(D + 8\eta_o A/abc)b/a + (D + 8\eta_o B/abc)a/b \\ & - 2(D + 8\eta_o C/abc)ab/c^2\} \cos\alpha \sin\alpha \\ & + \tfrac{1}{2}\{(D + 8\eta_o A/abc)b/a \\ & - (D + 8\eta_o B/abc)a/b\} \sin\alpha \cos\alpha \cos 2\phi \\ & + (8\eta_o H/abc - E) \sin\alpha \cos\alpha \sin 2\phi, \end{aligned} \tag{A15}$$

$$\begin{aligned} q_\phi^* = {} & \tfrac{1}{2}\{-(D + 8\eta_o A/abc)b/a \\ & + (D + 8\eta_o B/abc)a/b\} \sin\alpha \sin 2\phi \\ & + (8\eta_o H/abc - E) \sin\alpha \cos 2\phi, \end{aligned} \tag{A16}$$

$$\begin{aligned} q_n^* = {} & (D + 8\eta_o C/abc)ab/c^2 \\ & + \tfrac{1}{2}\{(D + 8\eta_o A/abc)b/a \\ & + (D + 8\eta_o B/abc)a/b \\ & - 2(D + 8\eta_o C/abc)ab/c^2\} \sin^2\alpha \\ & + \tfrac{1}{2}\{(D + 8\eta_o A/abc)b/a \\ & - (D + 8\eta_o B/abc)a/b\} \sin^2\alpha \cos 2\phi \\ & + (8\eta_o H/abc - E) \sin^2\alpha \sin 2\phi. \end{aligned} \tag{A17}$$

Fourier Coefficients of q_α^*, q_ϕ^*, q_η^*

$$\left.\begin{aligned} & q_{\alpha,0} = F \sin\alpha \cos\alpha,\ q_{\alpha,2} = G \sin\alpha \cos\alpha, \\ & q'_{\alpha,2} = L \sin\alpha \cos\alpha, \\ & q_{\phi,0} = 0,\ q_{\phi,2} = -G\sin\alpha,\ q'_{\phi,2} = L \sin\alpha, \\ & q_{n,0} = F \sin^2\alpha + (D + 8\eta_o C/abc)ab/c^2, \\ & q_{n,2} = G \sin^2\alpha,\ q'_{n,2} = L \sin^2\alpha, \end{aligned}\right\} \tag{A18}$$

where

$$\left.\begin{aligned} F = {} & \tfrac{1}{2}\{(D + 8\eta_o A/abc)b/a + (D + 8\eta_o B/abc)a/b \\ & - 2(D + 8\eta_o C/abc)ab/c^2\}, \\ G = {} & \tfrac{1}{2}\{(D + 8\eta_o A/abc)b/a - (D + 8\eta_o B/abc)a/b\}, \\ L = {} & 8\eta_o H/abc - E. \end{aligned}\right\} \tag{A19}$$

We are indebted to Mr. C. W. Boylan for his expert technical assistance in the execution of the rheoscope experiments.

This work was supported by research grant HL-12839 from the National Heart, Lung and Blood Institute.

Received for publication 3 April 1985 and in final form 10 February 1987.

REFERENCES

Barthès-Biesel, D., and H. Sgaier. 1985. Role of membrane viscosity in the orientation and deformation of a spherical capsule suspended in shear flows. *J. Fluid Mech.* 160:119–135.

Evans, E. A., and R. M. Hochmuth. 1978. Mechanochemical properties of membranes. *Curr. Top. Membr. Transp.* 10:1–63.

Evans, E. A., and R. Skalak. 1980. Mechanics and Thermodynamics of Biomembranes. CRC Press, Inc., Boca Raton, FL. Section 4.12.

Fischer, T. M., and H. Schmid-Schönbein. 1977. Tank-tread motion of red cell membrane in viscometric flow: behavior of intracellular and extracellular markers. *Blood Cells (Berl.).* 3:351–365.

Fung, Y. C. 1966. Theoretical considerations of the elasticity of red cells and small blood vessles. *Fed. Proc.* 25:1761.

Jeffery, G. B. 1922. The motion of ellipsoidal particles immersed in viscous fluids. *Proc. R. Soc. A.* 102:161–179.

Keller, S. R., and R. Skalak. 1982. Motion of a tank-treading ellipsoidal particle in a shear flow. *J. Fluid Mech.* 120:27–47.

Linderkamp, O., and H. J. Meiselman. 1982. Geometric, osmotic and membrane mechanical properties of density-separated red cells. *Blood.* 56:1121–1127.

Nash, G. B., and H. J. Meiselman. 1983. Red cell and ghost viscoelasticity. Effects of hemoglobin concentration and in vivo aging. *Biophys. J.* 43:63–73.

Novozhilov, V. V. 1964. Thin Shell Theory. P. Noordhoff, Ltd., Groningen, The Netherlands. Chapter 2, §33.

Secomb, T. W., and R. Skalak. 1982. Surface flow of viscoelastic membranes in viscous fluids. *Q. J. Mech. Appl. Math.* XXXV. 2:233–247.

Skalak, R. 1973. Modelling the mechanical behavior of red blood cells. *Biorheology.* 10:229–238.

Sutera, S. P., and R. Tran-Son-Tay. 1983. Mathematical model of the velocity field external to a tank-treading red cell. *Biorheology.* 20:267–282.

Sutera, S. P., R. Tran-Son-Tay, C. W. Boylan, J. R. Williamson, and R. A. Gardner. 1983. Study of variance in measurements of tank-treading frequency in populations of normal human red cells. *Blood Cells (Berl.).* 9:485–495.

Sutera, S. P., R. A. Gardner, C. W. Boylan, G. L. Carroll, K. C. Chang, J. S. Marvel, C. Kilo, B. Gonen, and J. R. Williamson. 1985. Age-related changes in deformability of human erythrocytes. *Blood.* 65:275–282.

Tran-Son-Tay, R. 1983. A study of the tank-treading motion of red blood cells in shear flow. D.Sc. dissertation, Department of Mechanical Engineering, Washington University, St. Louis, MO.

Tran-Son-Tay, R., S. P. Sutera, and P. R. Rao. 1984. Determination of RBC membrane viscosity from rheoscopic observations of tank-treading motion. *Biophys. J.* 46:65–72.